

## Experimental demonstration of a soft x-ray self-seeded free-electron laser

D. Ratner,<sup>1\*</sup> R. Abela,<sup>2</sup> J. Amann,<sup>1</sup> C. Behrens,<sup>1</sup> D. Bohler,<sup>1</sup> G. Bouchard,<sup>1</sup> C. Bostedt,<sup>1</sup> M. Boyes,<sup>1</sup> K. Chow,<sup>3</sup> D. Cocco,<sup>1</sup> F.J. Decker,<sup>1</sup> Y. Ding,<sup>1</sup> C. Eckman,<sup>1</sup> P. Emma,<sup>1</sup> D. Fairley,<sup>1</sup> Y. Feng,<sup>1</sup> C. Field,<sup>1</sup> U. Flechsig,<sup>2</sup> G. Gassner,<sup>1</sup> J. Hastings,<sup>1</sup> P. Heimann,<sup>1</sup> Z. Huang,<sup>1</sup> N. Kelez,<sup>1</sup> J. Krzywinski,<sup>1</sup> H. Loos,<sup>1</sup> A. Lutman,<sup>1</sup> A. Marinelli,<sup>1</sup> G. Marcus,<sup>1</sup> T. Maxwell,<sup>1</sup> P. Montanez,<sup>1</sup> S. Moeller,<sup>1</sup> D. Morton,<sup>1</sup> H.D. Nuhn,<sup>1</sup> N. Rodes,<sup>3</sup> W. Schlotter,<sup>1</sup> S. Serkez,<sup>4</sup> T. Stevens,<sup>3</sup> J. Turner,<sup>1</sup> D. Walz,<sup>1</sup> J. Welch,<sup>1</sup> J. Wu<sup>1</sup>

<sup>1</sup>SLAC, Menlo Park, California

<sup>2</sup>PSI, Villigen, Switzerland

<sup>3</sup>LBNL, Berkeley, California

<sup>4</sup>DESY, Hamburg, Germany and

\*dratner@slac.stanford.edu

The Linac Coherent Light Source (LCLS) has added self-seeding capability to the soft x-ray range using a grating monochromator system. We report demonstration of soft x-ray self-seeding with a measured resolving power of 2000-5000, wavelength stability of  $10^{-4}$ , and an increase in peak brightness by a factor of 2-5 across the photon energy range of 500-1000 eV. By avoiding the need for a monochromator at the experimental station, the self-seeded beam can deliver as much as 50 fold higher brightness to users.

The construction of x-ray free electron lasers (FELs) driven by self-amplified spontaneous emission (SASE) has pushed the brightness of x-ray sources by a remarkable ten orders of magnitude [1, 2]. Despite the relatively monochromatic output (typically bandwidth is on the order of 0.2-0.5% of the fundamental energy), many types of experiments benefit from even narrower bandwidth; the ability to target and measure fine energy structure in combination with femtosecond pulse length enables new opportunities in time-resolved x-ray spectroscopy. As an example, ultrafast resonant inelastic x-ray scattering (RIXS) can probe the evolution of low energy electronic excitations in correlated electron materials. At the Linac Coherent Light Source (LCLS), the soft x-ray (SXR) experimental hutch monochromator can select a narrow slice of the FEL bandwidth, but has diffraction efficiency of only 15-30% and increases the focal spot size, resulting in a factor of 10 or more drop in the total brightness [3]. Moreover some photon-hungry and time-resolved experiments cannot use a hutch monochromator and must accept the full SASE bandwidth. Rather than reducing the bandwidth after the FEL, it is preferable to reduce the FEL bandwidth itself.

The FEL amplification process ideally would begin from a well characterized, coherent 'seed.' However, due to a lack of external seeds at x-ray wavelengths, all current and planned x-ray FELs are SASE FELs, in which the shot noise of the electron beam itself generates the 'seed' [4]. Harmonic seeding techniques (e.g. [5]) can convert seeds to shorter wavelengths, but performance deteriorates at photon energies beyond a few hundred eV [6]. An alternative approach to external seeding is 'self-seeding,' in which the FEL is split into two pieces and a monochromatic slice of the spectrum from the first portion provides the seed for the second portion [7]. Self-seeding can be described as follows: First, the initial portion of the FEL generates relatively wide bandwidth SASE radiation. Second, a magnetic electron chicane

separates the electron and photon beams; on the photon branch, a tunable monochromator selects a narrow bandwidth out of the SASE spectrum, while on the electron branch the electron chicane dispersion resets the electron beam to its initial shot noise distribution (washing out microbunching from the SASE FEL). The chicane delay also matches the path lengths of the electron and photon beams so that they overlap following the seeding monochromator. Finally, the monochromatic x-rays and the electron beam then co-propagate in a second undulator line, restarting the FEL interaction from a narrow-bandwidth and near transform-limited seed.

Though originally studied for soft x-rays [8], a hard x-ray variant using a diamond Bragg condition has been in use at LCLS for the last two years [9, 10]. Following successful commissioning of the technically simpler hard x-ray self-seeding (HXRSS) system, a three-way collaboration between SLAC, Lawrence Berkeley National Lab, and the Paul Scherrer Institut formed to implement a grating-based soft x-ray self-seeding (SXRSS) project at LCLS [11]. Here we report the experimental demonstration of self-seeding in the soft x-ray range.

The LCLS SXRSS project was designed to fit into the existing LCLS undulator hall. To preserve SASE and HXRSS operation, only a single 3.4m undulator section could be replaced by the SXRSS components, requiring a compact design for both the seeding monochromator and chicane. The final design situated the SXRSS system in place of undulator #9, leaving as many as 8 undulators upstream of the seeding monochromator to generate the seed, and 23 downstream undulators to saturate and maximize the seeded FEL power.

The SXRSS system consists of an electron chicane and x-ray monochromator (Fig. 1), and a pair of beam overlap diagnostics (BODs) located further downstream. Here we give an overview of the system components, but a detailed description can be found in [12, 13]. The four-dipole electron chicane serves three purposes: steering

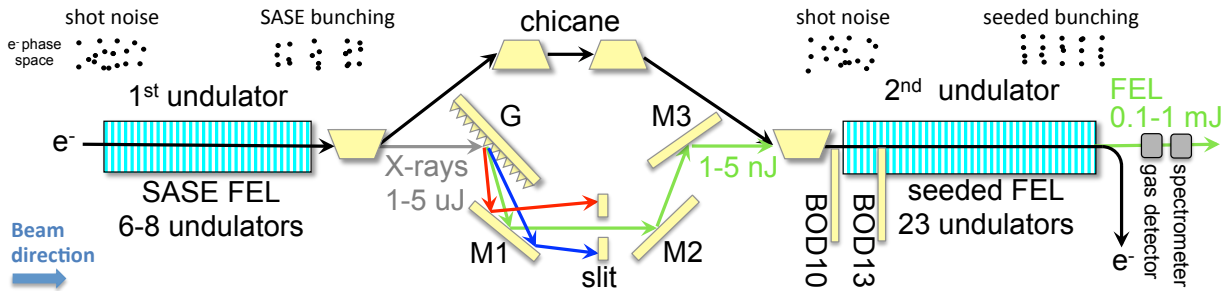


FIG. 1. Schematic of the SXRSS system (not to scale). Shot noise from randomly distributed electrons generates 1-5  $\mu\text{J}$  of relatively wide bandwidth SASE radiation in the first string of undulators (grey line). The seeding monochromator, consisting of a grating (G), three mirrors (M1, M2, M3), and an adjustable slit, selects a small bandwidth (green line) while the electron chicane directs the electron bunch around the monochromator and resets the electron beam to shot noise. Finally, the overlap diagnostics (BOD10 and BOD13) co-align electrons and monochromatic x-rays in the second half of the FEL. Pulse energies are shown for a nominal electron bunch with charge of 150 pC, and duration 100 fs, but other parameter ranges are also possible.

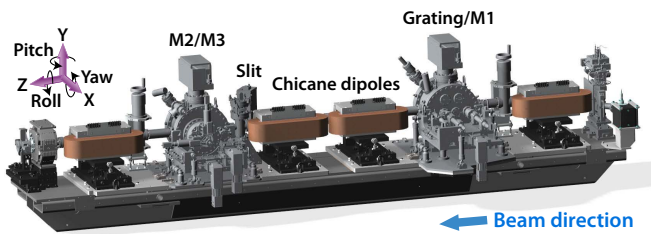


FIG. 2. CAD model of the final SXRSS design showing both the optics housing (Grating/M1, Slit, and M2/M3) and the electron chicane. In this figure, electrons move right to left to show the details of the optics chambers. The overlap diagnostics are further downstream.

electrons around the x-ray monochromator optics, delaying the electrons to match the x-ray delay in the seeding monochromator, and washing out microbunching from the initial SASE FEL. Due to the limited space available, the electron beam travels within a cm of the first and fourth x-ray optical surfaces. Rather than construct thin optics, a hole through the thick optical substrate provides safe passage of the electron beam through the optics [12]. The chicane can produce a maximum delay of approximately  $\sim 1$  ps, with a minimum delay of 0.5 ps in seeded mode to protect the optics. With a relative slice energy spread in the electron bunch of a few  $10^{-4}$ , the temporal dispersion of the chicane washes out any microbunching at x-ray wavelengths.

The seeding monochromator contains four Platinum-coated optical elements: a variable line spacing toroidal grating, two flat mirrors (M1 and M3), and a spherical mirror (M2) (Fig. 2). Motors insert or extract each optic remotely. A fifth element, a variable size slit, can be inserted between M1 and M2 to aid with alignment. (The slit is actually not needed while seeding, because only the narrow spectral slice that co-propagates with the electron beam can drive seeding. Effectively, the electron beam itself acts as a 'slit.')

The toroidal grating provides the dispersion of the monochromator, and

also focuses the beam vertically into undulator #10 and horizontally through the slit. The remotely adjustable pitch of M1 determines which wavelength passes through the monochromator along the electron beam path; M1 pitch is the only optic movement required to scan the seeded FEL x-ray wavelength. The final optics then focus (M2) and overlap (M3) the x-ray beam with the electron beam in undulator #10. Unlike hard x-ray self-seeding, where the seed passes directly through a diamond crystal, SXRSS requires transverse alignment of the x-rays and electrons. The slit and the two BODs help overlap the electron and photon beams and seed the FEL. Seeding is optimized by centering the seeded wavelength within the SASE bandwidth (M1 pitch), and maximizing both transverse overlap (grating Y, and M3 X, roll, and pitch), and temporal overlap (magnetic chicane strength) of the x-rays and electrons. Details of the overlap and alignment procedure are given in the appendix.

The power in the seed pulse must be sufficient to overcome SASE startup, but low enough to avoid damage to the optics. An estimated 0.15% of the SASE radiation incident on the grating is available for seeding, requiring at least  $1 \text{ mJ}/\text{cm}^2$  fluence at normal incidence for a nominal 100 fs, 2 kA electron bunch. Fluence above  $750 \text{ mJ}/\text{cm}^2$  can damage the grating, so the incident SASE is limited to  $30 \text{ mJ}/\text{cm}^2$  [14]. Though the damage threshold is acceptable for current operation, improvements may be necessary to avoid damage in a high-repetition rate machine. The damage considerations are described in more detail in the appendix.

A gas detector [15] and grating spectrometer [3] measure the final seeded FEL energy and spectrum, and both diagnostics can measure seeding at different positions along the undulator line [16]. The grating spectrometer, located in the SXR hutch, records single-shot seeded spectra with a resolution of  $\sim 100 \text{ meV}$  at 900 eV photon energy, beyond the expected resolving power of the seeding monochromator. Deep in saturation, the SASE FEL overtakes seeding, so it is preferable to setup seeding using only 10 of the 23 undulators down stream of

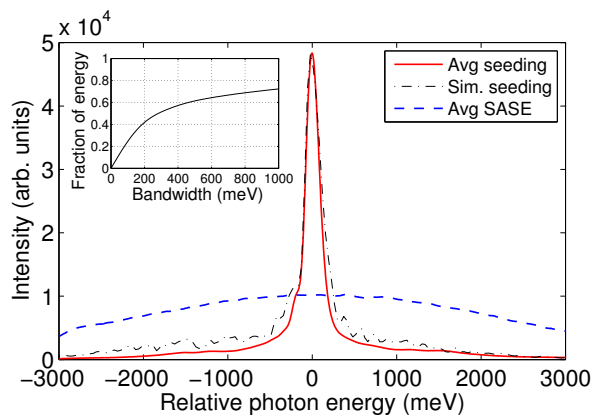


FIG. 3. Comparison of seeded (solid red line) and SASE (dashed blue line) spectra at 930 eV for 10,000 shot averages, and seeded simulation (sim.) averaged over 30 shots (dot-dashed black line). Both seeded and SASE spectra use the slotted foil to produce a 50 fs beam [18]. Seeded spectra are taken after undulator #25 and with the slit retracted. SASE spectra uses an optimized configuration with all undulators. Inset shows the fraction of FEL energy contained within an integrated bandwidth when seeding.

the seeding monochromator.

Self-seeding has been observed across the nominal photon energy range of 500-1000 eV, with typical performance described in Table I. Figure 3 shows a comparison between the seeded spectra and the optimized SASE configuration (all undulators, seeding optics extracted). Start-to-end Genesis simulations [17] agree with measurements. The seeded spectra exclude the final eight undulators, which primarily increase the undesirable SASE background. In the given spectra, the FWHM bandwidth of 175 meV contains approximately 40% of the total pulse energy. Some experiments may benefit from using the full undulator line, but the proportion of energy outside the seeding bandwidth will increase. Figure 4 shows SASE and seeded FEL gain, which matches simulations.

The peak brightness of the self-seeded FEL (defined as  $\text{mJ/s/m}^2/0.1\%$  bandwidth) is larger than that of optimized SASE by a factor of 2 to 5. For some narrow bandwidth applications, however, it is more relevant to compare the peak brightness of the full, unfiltered self-seeded beam with the brightness of the SASE beam filtered through a hutch monochromator. When including monochromator losses and focal size growth, the unfiltered seeded beam is up to 50 times brighter than the filtered SASE for the same FWHM bandwidth. Note that using the seeded beam without a hutch monochromator may require a setup with fewer undulator sections (to produce a cleaner spectrum) at the cost of reducing the final peak power by a factor of  $\sim 2$ .

The central SASE wavelength is determined by the electron energy, and the wavelength can jitter by as much as 0.4% shot-to-shot. By comparison, the seeded wavelength is determined by the M1 pitch, independent of the electron energy. Figure 5a shows single shot spectra,

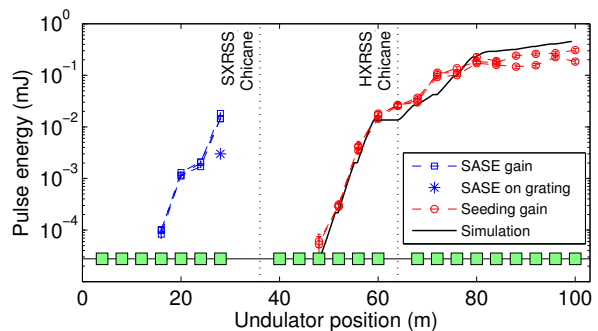


FIG. 4. Gain length scans showing SASE growth before the seeding monochromator (blue squares, 3 scans) and seeding growth afterwards (red circles, 3 scans). During seeded operation, undulator #1 is detuned to keep pulse energy on the grating below  $5 \mu\text{J}$  (blue star). Black line shows simulated seeding. Green boxes show undulators inserted during seeding; undulator #8 is removed to protect the grating, and undulators #9 and #16 were replaced by the self-seeding chicanes. Measured gain lengths for SASE ( $\sim 2 \pm 0.2$  m) and seeding ( $\sim 1.7 \pm 0.2$  m) match simulations. All measurements taken with the gas detector.

with shot-to-shot jitter of approximately 100 meV rms, corresponding to wavelength stability of  $10^{-4}$ . Though small compared to SASE, the jitter does broaden the average seeded spectrum: while the single shot bandwidth is 155 meV, wavelength jitter broadens the average bandwidth to 180 meV FWHM (Fig. 3). (Both values include corrections for the estimated 80 meV spectrometer bandwidth.) With a transmissive spectrometer upstream of the experimental station, it would be possible to remove the wavelength jitter by sorting shots in post-processing; a transmissive shot-by-shot spectrometer is currently under development. Possible causes of wavelength jitter include vibrations changing M1 pitch, transverse orbit fluctuations of the electrons (which change the seed wavelength), and changing electron phase space (which may alter the wavelength after seeding) [19]. Measured fluctuations in orbit ( $\sim 1 \mu\text{rad}$ ) and phase space ( $\sim 1 \text{ MeV/mm}$ ) are consistent with the observed jitter.

The seeded wavelength is fixed by the monochromator M1 angle, so the electron energy must be set such that the seeded wavelength is in the center of the FEL gain bandwidth. However, the electron energy jitters, and for many shots the seeding monochromator wavelength lies outside the gain region of the FEL and the electrons cannot be seeded. Figure 5b shows the total x-ray pulse energy as a function of measured electron bunch energy; for this example, 45% of the shots fall outside the FWHM of the seeded region. Efforts to reduce electron energy jitter are ongoing, and can potentially increase the average seeded power by a factor of 2. Considering only on-energy shots, the seeded pulse energy has 50% fluctuations, compared to 25% fluctuations for SASE. (Note that the SASE fluctuations in both cases were larger than usual due to the use of the slotted foil.)

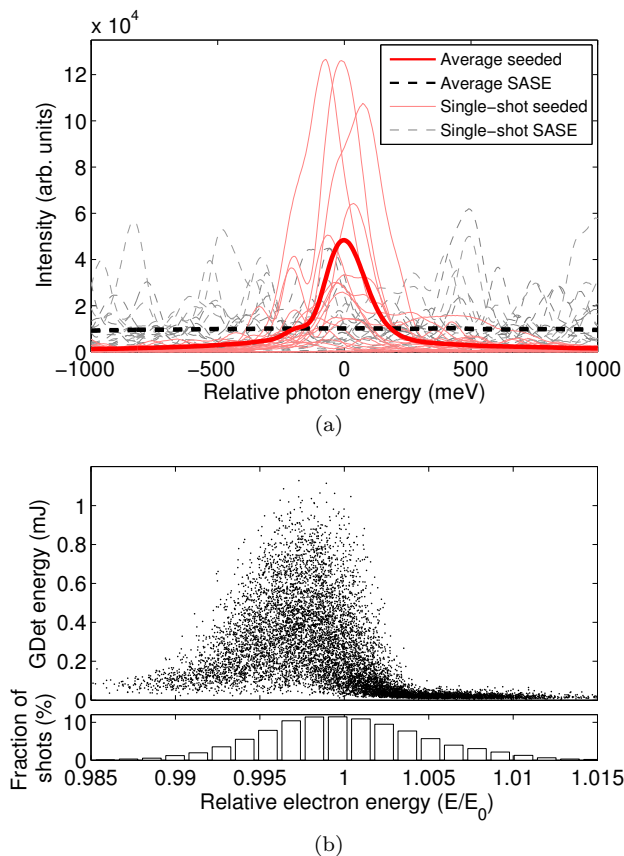


FIG. 5. Jitter of the seeded mode for 50 fs pulse at 930 eV. a) A comparison of 20 single-shot seeded (solid light red lines) and SASE (dashed grey lines) spectra shows fluctuations in both peak brightness and central seeded wavelength. Bold lines show average performance for both seeding and SASE. b) A ‘mustache’ scatter plot showing the FEL pulse energy from the gas detector (Gdet) vs. measured electron bunch energy for individual shots at 930 eV. (Average electron energy is 4.3 GeV.) Histogram at bottom shows the jitter of the central electron beam energy. The seeding monochromator was set slightly below the average electron energy to match the best lasing condition.

The seeding monochromator grating produces multiple order reflections, of which the first is strongest and used for self-seeding operation. The second order diffraction also has sufficient power to drive seeding. Despite having stronger dispersion, it does not provide higher resolving power due to diffraction effects, but in principle can access shorter wavelengths than the first order. By increasing M1 pitch angle in the seeding configuration, we have observed seeding driven by the second order, but have not tried to optimize second order seeding at this time.

Upgrades to the self-seeding mode will focus on improving performance after saturation and reducing the pedestal and shoulders of the seeded spectrum. At present the slit has been used primarily for alignment, but in principle with an optimized setup the narrow-

est slit (3  $\mu\text{m}$  wide) could increase the resolving power. Tapering beyond undulator #25 may require modifications to the undulator configuration. Two-color self-seeding has been demonstrated for the HXRSS system [20] and in principle two-color operation is also possible for SXRSS. However, unlike hard x-rays, simultaneous two-color operation at soft x-rays will require hardware changes. Two-color operation with only one color seeded is possible by detuning a portion of the undulators [21] or with two-bunch operation [22]. Seeded radiation with polarization control will be available following installation of the Delta undulators [23].

#### SXRSS performance

Photon energy range	500-1000 eV
SASE resolving power, average	$\sim 150$
SASE resolving power, single shot	$\sim 300$
Seeded resolving power	2000-5000
Seeded resolving power, single shot	2500-6000
Average power ratio: seeded vs. SASE	0.1-0.3
Maximum power ratio: seeded vs. SASE	$\sim 1$
RMS pulse energy jitter (on-energy shots)	50%
RMS pulse energy jitter (all shots)	100%
Brightness ratio: filt. seeded vs. filt. SASE	2-5
Brightness ratio: seeded vs. filt. SASE	20-50

TABLE I. Parameters of current seeding operation for a 50 fs pulse using the slotted foil [18]. SASE pulse energy assumes optimized, nominal operation with 50-100 fs pulse length. Brightness comparisons assume a hutch monochromator filters the SASE (‘filt.’). The seeded beam can be used directly or filtered by a hutch monochromator to remove shoulders.

Development of soft x-ray self-seeding will continue through 2015 as the SXRSS mode is prepared for user operation. As of August 2014, we have produced average resolving power of 2000-5000 with wavelength stability of  $10^{-4}$  across the designed energy range 500-1000 eV. Average brightness is approximately a factor of 2-5 higher and resolving power is approximately a factor of 20 higher than in optimized SASE configuration. Self-seeding without a hutch monochromator will provide a factor of 20 or more increase in brightness compared to SASE operation with a hutch monochromator. Future work will focus on improving electron stability to increase the average brightness, and reducing the pedestal of the x-ray spectrum to optimize user operation without a hutch monochromator. Taper studies are ongoing and simulations indicate an improved taper could increase brightness as well as peak power. Future work may eventually extend the operating range to 300-1200 eV.

#### ACKNOWLEDGMENTS

We would like to give special thanks for contributions from D. Van Campen, R. Follath, T. Rabedeau, S. Re-

iche, and S. Spielmann. Work at SLAC is supported by Department of Energy contract DE-AC02-76SF00515.

Work at LBNL part is supported by Department of Energy contract DE-AC02-05CH1123.

- 
- [1] P. Emma *et al.*, *Nature Photonics* **4**, 641 (2010).
  - [2] H. Tanaka *et al.*, *Nature Photonics* **6**, 540 (2012).
  - [3] P. Heimann *et al.*, *Review of Scientific Instruments* **82**, 093104 (2011).
  - [4] R. Bonifacio, C. Pellegrini, and L. M. Narducci, *Optics Communications* **50**, 373 (1984).
  - [5] L. H. Yu, *Phys. Rev. A* **44**, 5178 (1991).
  - [6] E. Allaria *et al.*, *Nature Photonics* **7**, 913 (2013).
  - [7] J. Feldhaus, E. L. Saldin, J. R. Schneider, E. A. Schneidmiller, and M. V. Yurkov, *Optics Communications* **140**, 341 (1997).
  - [8] Y. Feng, J. Hastings, P. Heimann, M. Rowen, J. Krzywinski, and J. Wu, in *Proceedings of the 2010 FEL Conference* (Malmö City, Sweden, 2010).
  - [9] G. Geloni, V. Kocharyan, and E. Saldin, *Journal of Modern Optics* **58**, 1391 (2011).
  - [10] J. Amann *et al.*, *Nature Photonics* **6**, 693 (2012).
  - [11] Y. Feng *et al.*, in *Proceedings of the 2012 FEL Conference* (Nara, Japan, 2012).
  - [12] D. Cocco *et al.*, *Proc. SPIE* **8849**, 88490A (2013).
  - [13] H. Loos, P. Montanez, D. Ratner, and J. Hastings, *LCLS Physics Specifications for the SXRSS Beam Overlap Diagnostics*, Report SLAC-PUB-16073 (SLAC, 2014).
  - [14] J. Krzywinski, D. Cocco, S. Moeller, and D. Ratner, *Damage threshold of platinum coating used for optics for self-seeding of Soft X-ray Free Electron Laser*, Report SLAC-PUB-16096 (SLAC, 2014).
  - [15] S. P. Hau-Riege, R. M. Bionta, D. D. Ryutov, and J. Krzywinski, *J. Appl. Phys.* **103**, 053306 (2008).
  - [16] D. Ratner *et al.*, in *Proceedings of the 2009 FEL Conference* (2009).
  - [17] S. Reiche, *Nucl. Instrum. Meth. A* **429**, 243 (1999).
  - [18] P. Emma, K. Bane, M. Cornacchia, Z. Huang, H. Schlarb, G. Stupakov, and D. Walz, *Phys. Rev. Lett.* **92**, 074801s (2004).
  - [19] A. Marinelli, C. Pellegrini, L. Giannessi, and S. Reiche, *Phys. Rev. ST Accel. Beams* **13**, 070701 (2010).
  - [20] A. A. Lutman *et al.*, *Phys. Rev. Letters* **113**, 254801 (2014).
  - [21] A. A. Lutman, R. Coffee, Y. Ding, Z. Huang, J. Krzywinski, T. Maxwell, M. Messerschmidt, and H.-D. Nuhn, *Phys. Rev. Lett.* **110**, 134801 (2013).
  - [22] A. Marinelli *et al.*, Submitted for publication (2014).
  - [23] H.-D. Nuhn *et al.*, in *Proceedings of the 2013 FEL Conference* (New York, New York, 2013) pp. SLAC-PUB-15743.
  - [24] T. Koide *et al.*, *Applied Optics* **26**, 3884 (1987).
  - [25] S. Serkez, J. Krzywinski, Y. Ding, and Z. Huang, in *Proceedings of the 2014 FEL Conference* (Basel, Switzerland, 2014) p. MOP90.

## Appendix A: Alignment of X-rays and electrons

The primary challenge for the soft x-ray self-seeding project, in particular compared to hard x-ray self-seeding, is the need to overlap the x-rays and electrons

transversely. The beam overlap diagnostics (BODs) are used to measure the transverse positions of both beams. The first diagnostic (BOD10) sits between the seeding monochromator and undulator #10. Ideally, the second diagnostic would follow undulator #10, but there is not sufficient room at that location, so instead the diagnostic (BOD13) sits in the long gap between undulators #12 and #13. Each BOD consists of a pair of crossed carbon wires (40  $\mu\text{m}$  thick) and a YAG screen (20  $\mu\text{m}$  thick to reduce radiation). The design is shown in Fig. 6. The electron beam position is found by moving the wires through the electron beam while measuring current loss downstream. To locate the x-ray beam, a camera images the fluorescence generated by the x-ray beam when incident on the 10 mm wide YAG screen (Fig. 7). The camera also images the two wires to determine the separation between the electron and photon beams. Note that the synchrotron stripe from the electrons in the final chicane bend magnet can be used for vertical alignment of the x-rays and electrons without an additional scan of the electron wires. After finding both x-ray and electron positions, a measured response matrix determines the required optics changes for overlap. To overlap the beam in position and angle, vertically and horizontally, requires four degrees of freedom, provided by grating Y position, and M3 X position, roll, and pitch. Note that M1 pitch angle changes the wavelength, but does not affect alignment [12]. To avoid hitting the YAG with the electron beam, the screen sits 1.5 mm to the side of the electron beam; moving M3 pitch by  $\sim 1$  mrad redirects the x-rays to intersect the screen. Technical details of the BOD design can be found in [13].

A total of 9 remotely controlled motors operate the SXRSS monochromator. The motors control positions of grating/M1 X (#1), grating Y (#2), M1 pitch (#3), slit Y (#4), slit X (#5), M2 X (#6), M3 X (#7), M3 pitch (#8), and M3 roll (#9). Motors #1, #6, and #7 insert the grating, M1, M2, and M3 optics, and the motor #4 inserts the slit. The slit Y motion also controls the slit size, and M1 pitch determines the seed wavelength. The rest of the motors (along with #7) align the x-rays.

Initial alignment of the optics proceeded sequentially, starting with alignment of the grating, and finishing with M3. To set the grating position, the beam was imaged on a YAG screen surrounding the slit (YAGSLIT). The transmitted intensity on YAGSLIT as a function of grating X-position gives the horizontal (X) alignment of the grating. With M2 and M3 in the OUT position, the diffracted x-ray beam passes directly to BOD10. M1 pitch and horizontal slit position are both set so that the x-rays pass through the slit and intersect BOD10 displaced by 3.8 mm from the electron beam (to keep

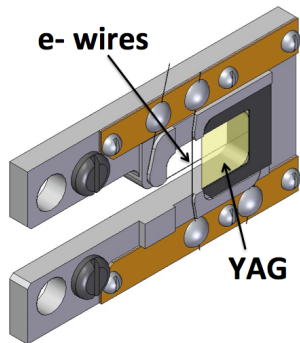


FIG. 6. Diagram of BOD design. The YAG screen images the x-ray beam, and the wires are scanned through the electron beam to measure the electron position. Both YAG and electron wires are imaged by the same camera to determine the relative positions.

the x-rays parallel to the electron beam). The grating vertical position is set empirically by overlapping the x-rays with the synchrotron stripe of the electrons (Fig. 7). With the grating and M1 aligned, M2 is inserted until it blocks the x-rays, which determines the correct M2 horizontal position. Finally, M3 is inserted and the overlap procedure sets the correct M3 horizontal (X) position, pitch, and roll, and grating Y position. Note that except for the grating vertical (Y) and M3 positions (which are used to steer the x-rays vs. the electrons), and M1 pitch (which selects wavelength) all other optics remain fixed after the initial alignment.

The x-ray signal on the BOD YAGs is obscured by strong coherent radiation generated by the electrons. Imaging is still possible by taking backgrounds while blocking only the x-ray beam and by keeping the screen at least 1.5 mm from the electrons to reduce the coherent radiation power. The most challenging measurement is of the horizontal x-ray position at BOD13, but the 15  $\mu\text{m}$  slit between M1 and M2 isolates the narrow slice of x-rays used for seeding, and facilitates measurement on BOD13 (Fig. 8). After transverse alignment of x-rays and electrons, temporal overlap is achieved by scanning the electron chicane strength, just as for the hard x-ray case. A discrepancy of 50-100 fs (shorter electron delay than expected) has not been understood to this time.

## Appendix B: Grating damage concerns

Damage to the platinum coated optics is a major concern for SXRSS operation. The optical surface of the grating was chosen to be platinum rather than boron carbide to allow oxygen cleaning of the optics as necessary [24], but as a result the optical surface is more sensitive to radiation damage. Damage can result from both the average seed intensity, as well as single shots; in the unsaturated regime, fundamental SASE variations cause the single-shot power to spike six fold higher than

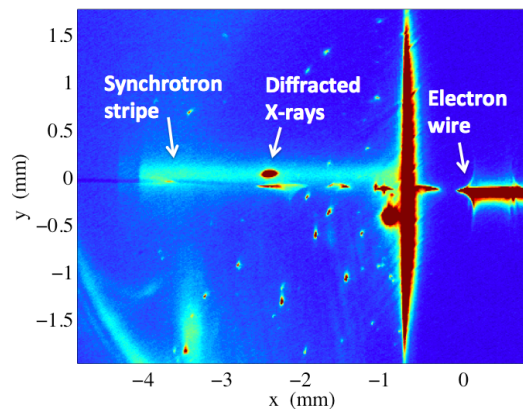


FIG. 7. Diffracted x-rays through the 15  $\mu\text{m}$  slit visible on BOD10. The synchrotron stripe from the electrons exiting the chicane can be used for vertical alignment.

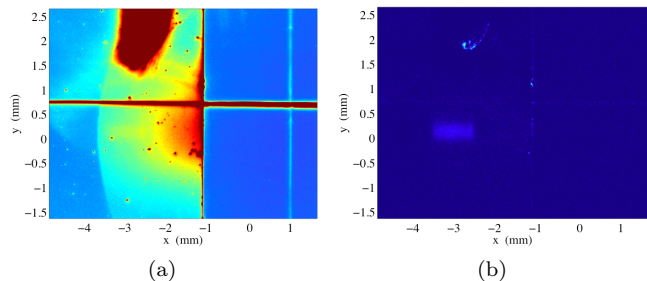


FIG. 8. Averaged image of x-rays on BOD13 before (a) and after (b) background subtraction. Before background subtraction (left) x-rays on BOD13 are overwhelmed by coherent radiation from the electron beam. After taking backgrounds with only the x-rays blocked (by intentionally deflecting the beam with M1 pitch) it is possible to observe the x-rays (right). The beam would normally fill the entire beam pipe, but a 15  $\mu\text{m}$  slit allows X position measurement also.

the average power.

To determine safe power levels, damage studies of platinum coated optics were carried out prior to final coating of the grating. Multi-shot damage was observed at 750  $\text{mJ}/\text{cm}^2$  average fluence (normal to the beam direction). In the unsaturated regime, SASE fluctuations cause the power to spike six fold higher than the average power, so single-shot damage is also relevant and needs further study. To reduce the fluence during operation, we typically extract undulator #8 to expand the x-ray beam size at the grating. A comparison of the damage threshold to operational requirements is shown in Fig. 9 and details can be found in [14]. To determine the minimum fluence for seeding, we propagate the SASE pulse through the optics [25] to seed a Genesis simulation [17] on a start-to-end electron beam. We define the minimum fluence from the initial energy required such that the integrated seeded FEL pulse energy at saturation is a factor of 3 higher than the integrated SASE pulse energy (solid black line in Fig. 9).

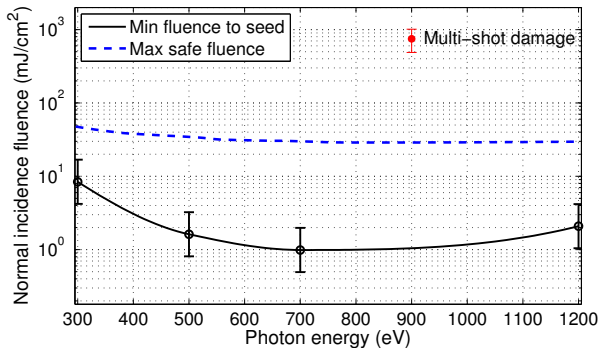


FIG. 9. From simulations, a minimum level of fluence (black line, nominal 50 fs, 1.5 kA pulse) is required incident on the grating so that the seed outcompetes SASE after the seeding monochromator. To protect the grating in operation, the maximum fluence on the grating (dotted blue line) is set well below the measured 750 mJ/cm<sup>2</sup> multi-shot damage level. The maximum allowed fluence at 700 eV is equivalent to 1.25  $\mu$ J with undulator #8 inserted or 5  $\mu$ J with undulator #8 removed.

During operation, pulse energy on the grating is determined by extracting the seeding monochromator optics and downstream undulators and measuring the total energy with the gas detectors [15]; when set to high gain, the gas detectors can measure down to the 100 nJ level. Because energy cannot be measured during operation, and in principle may increase without operator knowledge, the maximum fluence allowed on the grating is set a factor of 25 below the expected multi-shot damage threshold (dotted blue line, Fig. 9). The maximum fluence at 700 eV with undulator #8 extracted corresponds to 5  $\mu$ J. The first undulators are removed as necessary to achieve a safe power level. Removing a single undulator can reduce power by more than a factor of 5, so fine-tuning of the seed energy is accomplished by intentionally detuning the first inserted undulator. The seeding data shown in the Letter were obtained with undulator #8 extracted, and with the K value of undulator #1 detuned by 0.4%. Parameters used for seeding are summarized in Table II.

In addition to the pulse energy limits, a boron carbide

'chin guard' protects the side of the grating (normal to the beam direction) from spontaneous radiation of up to 20 mW. A copper braid conducts heat from the grating to the optics housing to protect the optic from overheating. We note that while heating is relatively small at LCLS, future high repetition rate machines will require new advances to protect the optics from both SASE and spontaneous heating.

### Appendix C: Diagnostics

A gas detector [15] and grating spectrometer [3] measure the final seeded FEL energy and spectrum. Both

Conditions for seeding results	
Photon energy	930 eV
Pulse length	50 fs
Peak current	2 kA
Undulator configuration, before mono.	1-7 IN, 8 OUT
Undulator configuration, after mono.	10-25 IN, 26-33 OUT
Pulse energy at grating	4 $\mu$ J
Seed power after mono.	10 kW

TABLE II. Parameters of seeding results presented in this Letter. Seed power refers to the power interacting with the electrons after the SXRSS monochromator (mono.)

detectors are situated following the undulators, but by either removing undulators or introducing an electron orbit oscillation within the undulator, it is possible to halt the FEL process early and conduct power measurements at any location along the undulator [16]. The grating spectrometer, located in the SXR hutch, has a high resolution 2001/mm grating which is capable of resolving SASE spikes of width  $\sim$  80 meV; this is better than the resolving power of the seeding monochromator, but is close enough to bias the measurement. As a result, quoted bandwidths assume a Gaussian spectrum with the hutch spectrometer resolution subtracted in quadrature. A lower resolution 1001/mm grating is also available for photon energies below 800 eV.